J Electr Eng Technol.2018; 13(5): 2125-2133
http://doi.org/10.5370/JEET.2018.13.5.2125

ISSN(Print) 1975-0102
ISSN(Online) 2093-7423

A Robust Adaptive Control for Permanent Magnet Synchronous Motor Subject to Parameter Uncertainties and Input Saturations

Shaofang Wu† and Jianwu Zhang*

Abstract – To achieve high performance speed regulation, a robust adaptive speed controller is proposed for the permanent magnet synchronous motor (PMSM) subject to parameter uncertainties and input saturations in this paper. A nonlinear adaptive control is introduced to compensate the PMSM speed tracking errors due to uncertainties, disturbances and control input saturation constraints. By combining the adaptive control and the nonlinear robust control based on the interconnection and damping assignment (IDA) strategy, a new robust adaptive control is designed for speed regulation of PMSM. Stability and robustness of the closed-loop control system involved with the constrained control inputs rather than unconstrained control inputs are validated. Simulations for PMSM control in the presence of uncertainties and saturations nonlinearities show that the proposed approach is effective to regulate speed, and the average tracking error using the proposed approach is at least 32% smaller than the compared methods.

Keywords: Permanent magnet synchronous motor, Robust control, Adaptive control, Parameter uncertainties, Input saturations.

1. Introduction

An increasing use of permanent magnet synchronous motor (PMSM) is found in robotics, vehicle and transmission drives in recent years due to PMSM's high efficiency, high power density and wide speed range. PMSM is a nonlinear time-varying and strong-coupled dynamic system. Parameter variations and external perturbations are unavoidable effects in the PMSM drives [1-3]. In addition, the control input saturation, for example voltage saturations in the rapid acceleration operation of PMSM drive, is also a very common nonlinear phenomenon in the PMSM control system [4].

The conventional proportional-integral (PI) or PI-derivative (PID) regulators are widely used in the industrial practices. But the PID controls, based on the specified model parameters and the time separation assumption, cannot provide guaranteed stability if uncertainties, load changes and input saturation constraints exist [5-6].

In the recent decades, researchers have designed considerable advanced controls for the PMSM drives to overcome drawbacks of the conventional controllers and thus obtain better performances. A robust predictive controller is proposed by Türker et al. [7] to realize PMSM control. A nonlinear robust control using adaptive backstepping technique is proposed by Garin et al. [8] to achieve wide range speed regulation. The robust control with T-S fuzzy model is used to implement robust PMSM control [9-11]. A model reference adaptive control (MRAC) is proposed for the PMSM control, where the neural network is employed to deal with the nonlinear characteristics [12]. The robust control using the wavelet-neural-network for the motor subject to the parameter variations, is proposed to attenuate the disturbances and improve control performances [13-15]. And a sliding-mode control which employs a wavelet-neural-network to predict uncertainties on-line is proposed [16]. However, designs of the basis wavelet functions and trainings of the networks require empirical skills, prior system knowledge and a great computational capacity.

The works introduced above are proposed to realize the robust control for PMSM regarding uncertainties. The input saturation constraints, which would degrade the control performances or even induce instability, have not been considered. A stabilization method for locally Lipschitz nonlinear systems with saturation is presented in [17]. The PI controller is used to handle the effect of integrator windup when large set-point changes are made in the PMSM control [18-19]. Another of these works proposed a nonlinear predictive control (NPC) to compensate for the windup nonlinearities [20-21]. To deal with the constraints, the NPC approach reduces to a PI-type compensation. And this PI-type approach is used to restrict current overshooting, rather than handling the control input saturations.

The interconnection and damping assignment (IDA) strategy is used in the PMSM control [6, 22, 23], but problems of robustness to disturbance and saturations are not considered. Moreover, the adaptive control in the port-

† Corresponding Author: National Engineering Laboratory for Automotive Electronics and Control Technology, Shanghai Jiaotong University, Shanghai, China. (shaofangwu@sjtu.edu.cn)
* National Engineering Laboratory for Automotive Electronics and Control Technology, Shanghai Jiaotong University, Shanghai, China.
Received: November 12, 2017; Accepted: May 23, 2018

controlled Hamilton system with dissipation (PCHD) is used to compensate uncertainties and disturbances and thus improve performances [24-26]. The nonlinear robust technique is proposed to deal with the stabilization problem using the local polyhedral representation of saturations [27].

Instead of using the heuristic local representation of the actuator saturations, this paper incorporates a new adaptive compensation with the nonlinear robust control to address the parameter uncertainties and input saturations and achieve high-performance PMSM speed control. Verification is provided for the closed-loop stability. This paper is organized as follows. Section 2 describes the PMSM model, followed by the adaptive designs in Section 3. Section 4 presents the nonlinear robust control designs. Simulations are conducted in Section 5. And Section 6 concludes the paper.

2. Mathematical Modelling of PMSM Drives

By considering parameter uncertainties, external disturbances and control input saturation effects, the model for PMSM in the synchronously rotating direct-quadrature (d-q) reference frame can be presented as follows [20]

$$\begin{cases} L_d \dot{i}_d = -R_s i_d + \omega_e L_q i_q + \Delta_d + sat(u_d) + w_1 \\ L_q \dot{i}_q = -R_s i_q - \omega_e L_d i_d - \omega_e \psi + \Delta_q + sat(u_q) + w_2 \\ \frac{J_m}{n_p}\dot{\omega}_e = T_e - \frac{B}{n_p}\omega_e - T_L + \Delta_\omega + w_3 \end{cases} \quad (1)$$

where i_d and i_q are stator currents in the d- and q-axis, ω_e is electrical angular velocity of rotor; u_d and u_q are voltages in the d- and q-axis, L_d and L_q are inductances in the d-q frame, R_s is stator resistance, B is coefficient of friction, and ψ is the permanent magnet flux linkage, n_p is number of pole pairs, J_m is moment of inertia, T_L and $T_e = n_p[\psi i_q + (L_d - L_q) i_d i_q]$ are the load and electromagnetic torque. $\Delta_{\mathrm{f}} = [\Delta_d, \Delta_q, \Delta_\omega]^{\mathrm{T}}$ is the unknown vector function denoting uncertainties due to changes of motor parameters. And, $\mathbf{w} = [w_1, w_2, w_3]^{\mathrm{T}}$ is external disturbance vector. $sat(u_i)$ means the effective control input with the nonlinear saturation function $sat(\cdot)$. The input nonlinearity is given as follows

$$sat(u_i) = \begin{cases} u_i^{\max}, u_i > u_i^{\max} \\ u_i, u_i^{\min} \le u_i \le u_i^{\max} \\ u_i^{\min}, u_i < u_i^{\min} \end{cases} \quad (2)$$

where $i = d, q$. $u_i^{\min}$ and $u_i^{\max}$ are the output limits of the actuator. It is indicated by (2) that the control inputs are limited by the saturation constraints.

To facilitate the nonlinear robust and adaptive control design, (1) is rewritten in the following form as

$$\begin{cases} \dot{\mathbf{x}} = [\mathbf{J}(\mathbf{x}) - \mathbf{R}(\mathbf{x})]\nabla H(\mathbf{x}) + \Delta_{\mathrm{f}} + \mathbf{g}_1(\mathbf{x})\bar{\mathbf{u}} + \mathbf{g}_2(\mathbf{x})\mathbf{w} \\ \mathbf{y} = \mathbf{g}_2^{\mathrm{T}}\nabla H(\mathbf{x}) \end{cases} \quad (3)$$

where $\mathbf{x} = [x_1, x_2, x_3]^{\mathrm{T}} = [L_d i_d, L_q i_q, \frac{J_m}{n_p}\omega_e]^{\mathrm{T}}$ is the state vector, $\bar{\mathbf{u}} = [sat(u_d), sat(u_q), -T_L]^{\mathrm{T}}$ is the system input, $\mathbf{y}$ is the system output.

$$\mathbf{J}(\mathbf{x}) = -\mathbf{J}^{\mathrm{T}}(\mathbf{x}) = \begin{bmatrix} 0 & 0 & n_p x_2 \\ 0 & 0 & -n_p(x_1 + \psi) \\ -n_p x_2 & n_p(x_1 + \psi) & 0 \end{bmatrix}, \text{ and}$$

$\mathbf{R}(\mathbf{x}) = \mathbf{R}^{\mathrm{T}}(\mathbf{x}) = diag\{R_s, R_s, B\}$ are the interconnection and dissipation matrices. $\mathbf{g}_1(\mathbf{x}) = \mathbf{g}_2(\mathbf{x}) = diag\{1,1,1\}$ are the input gain matrices. $H(\mathbf{x}) = \frac{1}{2}\mathbf{x}^{\mathrm{T}}\mathbf{D}^{-1}\mathbf{x}$ is the Hamiltonian function with $\mathbf{D} = diag\{L_d, L_q, \frac{J_m}{n_p}\}$.

3. Adaptive Compensations to Parameter Uncertainties and Input Saturations

To compensate effects of parameter uncertainties and input saturation constraints of PMSM drive systems, the adaptive strategies are designed.

3.1 Nonlinear adaptive compensations to uncertainties

An adaptive compensation term, which is constructed using the nonlinear matched function related to the system states, is added to the control actions to counteract the errors caused by parameter uncertainties. To describe the parameter uncertainties of the PMSM control system, a commonly-used matched assumption is given below.

Assumption 1 [18]

There exist $\mathbf{\Phi}(\mathbf{x}) = \mathbf{\Phi}^{\mathrm{T}}(\mathbf{x}) \in \mathbb{R}^3$ such that

$$\Delta_{\mathrm{f}} = \mathbf{g}_1(\mathbf{x})\mathbf{\Phi}^{\mathrm{T}}(\mathbf{x})\boldsymbol{\theta} \quad (4)$$

where $\boldsymbol{\theta} \in \mathbb{R}^3$ is an unknown vector. According to this description, the adaptive term can be designed for the estimation and compensation of the control errors.

Remark 1

As a matched condition, Assumption 1 is common in the adaptive control of uncertain systems [22, 26]. And in PMSM control, parameter uncertainties due to changes of resistances, inductances, etc., can be represented by a function with unknown vector.

3.2 Nonlinear adaptive compensations to control input saturation constraints

The voltages, as the control inputs in PMSM control, are limited by a given dc-link voltage u_{dc}. The voltage actions

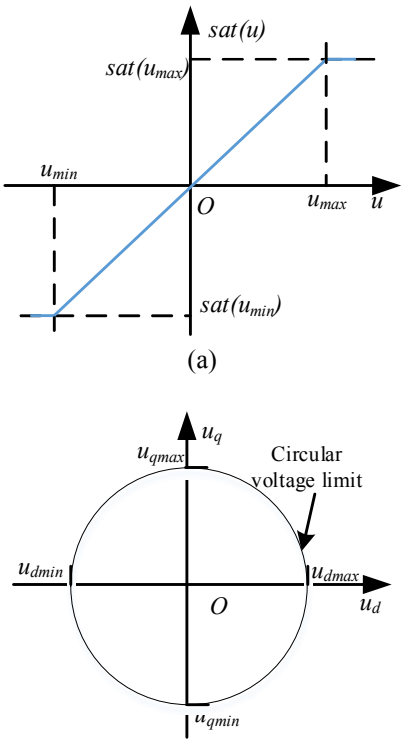

Fig. 1. Voltage saturations in PMSM control: (a) input saturation; (b) control voltage constraints

would become saturated when the expected voltages exceed the limits of saturation, as depicted in Fig. 1(a). In the synchronously rotating d-q frame, the control voltages, u_d and u_q, and are constrained in the circular voltage limit as shown in Fig. 1(b). As shown in Fig. 1(b), voltage constraints for the surface-mount PMSM (SPMSM) control are determined by the voltage limits. The circle voltage limitation can be expressed as the following form

$$u_d^2 + u_q^2 \le u_{s\max}^2 = u_{dc}^2 \tag{5}$$

where $u_{s\max}$ is the maximum radius of the voltage circle. Because it is difficult to solve this kind of nonlinear constraints in the control loop, another representation the saturation constraint is introduced by considering the operation characteristics of PMSMs. Limits of voltages u_d and u_q in the steady-state operation of PMSMs can be presented in the following form

$$\begin{cases} u_{d\lim} = -\omega_T L_q i_q \\ u_{q\lim} = \omega_T (L_d i_d + \psi) \end{cases} \tag{6}$$

where $u_{d\lim}$ and $u_{q\lim}$ represent voltage limits in the d- and q-axis, ω_T is the turning velocity of the motor and can be approximated by the nominal velocity of the motor ω_N. Using the parameters given in the machine design, voltage limits in d- and q-axis can be calculated with (6) while ensuring that the motor operates in the MTPA or i_d =0 strategy.

Remark 2

Only i_d =0 control for SPMSM is discussed in this paper, and the flux-weakening operation has not been included yet.

To describe the saturation constraints, let $\boldsymbol{\psi}^{\mathrm{T}}(\mathbf{x})\boldsymbol{\eta} = \mathbf{u} - sat(\mathbf{u})$, that is $sat(\mathbf{u}) = \mathbf{u} - \boldsymbol{\psi}^{\mathrm{T}}(\mathbf{x})\boldsymbol{\eta}$, where $\boldsymbol{\psi}(\mathbf{x}) = \boldsymbol{\psi}^{\mathrm{T}}(\mathbf{x}) \in \mathbb{R}^{3\times 3}$ and $\boldsymbol{\eta}$ are function matrix and unknown vector. Then, the saturation compensations can be constructed using the adaptive strategy as follows

$$\dot{\hat{\boldsymbol{\eta}}} = -\mathbf{P}\boldsymbol{\psi}(\mathbf{x})\mathbf{g}_1^{\mathrm{T}}(\mathbf{x})\nabla H_d(\mathbf{x}) \tag{7}$$

where $H_d(\mathbf{x})$ is a new closed-loop energy function, which would be further explained later.

If the saturation occurs, the adaptive action would arise naturally to compensate the effects.

4. Nonlinear Robust Control Design

4.1 The IDA control formulation

The PCHD is given in the general form as [28]

$$\dot{\mathbf{x}} = [\mathbf{J}(\mathbf{x}) - \mathbf{R}(\mathbf{x})]\nabla H(\mathbf{x}) + \mathbf{g}_1(\mathbf{x})\mathbf{u} \tag{8}$$

The analytical feedback control for (8) may be rewritten in the special form as [6, 24]

$$\begin{aligned} \dot{\mathbf{x}} &= [(\mathbf{J} + \mathbf{J}_a) - (\mathbf{R} + \mathbf{R}_a)]\nabla H_d(\mathbf{x}) \\ &= [\mathbf{J}_d - \mathbf{R}_d]\nabla H_d(\mathbf{x}) \end{aligned} \tag{9}$$

where $H_d(\mathbf{x})$ is the new closed-loop energy function. $\mathbf{J}_d$ and $\mathbf{R}_d$ are the new interconnection and dissipation matrices. $\mathbf{J}_a$ and $\mathbf{R}_a$ are interconnection and dissipation matrices decided by the control inputs.

The required load torque can be estimated by observer, and the equilibrium states can be given as [6, 29] $\mathbf{x}^* = [L_d i_d^*, L_q i_q^*, \frac{J_m}{n_p}\omega_e^*]^{\mathrm{T}}$. Then, selecting $\mathbf{x}_e = \mathbf{x} - \mathbf{x}_e^*$, $H_d(\mathbf{x}) = \frac{1}{2}\mathbf{x}_e\mathbf{D}^{-1}\mathbf{x}_e$ and appropriate matrices $\mathbf{J}_a(\mathbf{x})$ and $\mathbf{R}_a(\mathbf{x})$, the control actions to derive (8) into (9) can be obtained without the need to solve a set of partial differential equations [6, 28, 30]. The control actions are given as [6, 29]

$$\mathbf{u}_1 = -\mathbf{k}_1\mathbf{g}_1(\mathbf{x})\nabla H_d(\mathbf{x}) + \mathbf{b}^* \tag{10}$$

where $\mathbf{k}_1 \in \mathbb{R}^{3\times 3}$ is a positive semi-definite matrix to shape the new system and guarantee its stability, $\mathbf{b}^*$ is related to the command and external load and used to modify the equilibrium states. This control action would be further incorporated with the full control design.

4.2 Robust control law design

The penalty signal for nonlinear robust design is given as [28].

$$\mathbf{z} = \mathbf{r}(\mathbf{x})\mathbf{g}_1^{\mathrm{T}}(\mathbf{x})\nabla H_d(\mathbf{x}) + t(\mathbf{x})\bar{\mathbf{u}} \tag{11}$$

By combining (3) with (11), the nonlinear robust control formulation can be presented as (12). Here, it can be set that $\mathbf{r}(\mathbf{x})$ is full column rank matrix and $t(\mathbf{x})$ is zero.

$$\begin{cases} \dot{\mathbf{x}} = [\mathbf{J}(\mathbf{x}) - \mathbf{R}(\mathbf{x})]\nabla H(\mathbf{x}) + \Delta_{\mathrm{f}} + \mathbf{g}_1(\mathbf{x})\bar{\mathbf{u}} + \mathbf{g}_2(\mathbf{x})\mathbf{w} \\ \mathbf{y} = \mathbf{g}_2^{\mathrm{T}}(\mathbf{x})\nabla H(\mathbf{x}) \\ \mathbf{z} = \mathbf{r}(\mathbf{x})\mathbf{g}_1^{\mathrm{T}}(\mathbf{x})\nabla H_d(\mathbf{x}) + t(\mathbf{x})\bar{\mathbf{u}} \end{cases} \tag{12}$$

For the PMSM control system (12), the robust adaptive control law is designed as

$$\begin{cases} \mathbf{u} = -\mathbf{k}_1\mathbf{g}_1(\mathbf{x})\nabla H_d(\mathbf{x}) + \mathbf{b}^* - \boldsymbol{\Phi}^{\mathrm{T}}\hat{\boldsymbol{\theta}} + \boldsymbol{\psi}^{\mathrm{T}}\hat{\boldsymbol{\eta}} \\ \quad\quad - \mathbf{k}_2(\frac{1}{2}\mathbf{r}^{\mathrm{T}}\mathbf{r} + \frac{1}{2\gamma^2})\mathbf{g}_1(\mathbf{x})\nabla H_d(\mathbf{x}) \\ \dot{\hat{\boldsymbol{\theta}}} = \mathbf{Q}\boldsymbol{\Phi}(\mathbf{x})\mathbf{g}_1^{\mathrm{T}}(\mathbf{x})\nabla H_d(\mathbf{x}) \\ \dot{\hat{\boldsymbol{\eta}}} = -\mathbf{P}\boldsymbol{\psi}(\mathbf{x})\mathbf{g}_1^{\mathrm{T}}(\mathbf{x})\nabla H_d(\mathbf{x}) \end{cases} \tag{13}$$

where $\mathbf{k}_2 = \mathbf{k}_2^{\mathrm{T}} \in \mathbb{R}^{3\times 3}$ is positive semi-definite gain matrix to attenuate the external disturbances; $\mathbf{P} \in \mathbb{R}^{3\times 3}$ and $\mathbf{Q} \in \mathbb{R}^{3\times 3}$ are positive definite symmetric adaption gains; $\boldsymbol{\Phi}^{\mathrm{T}}\hat{\boldsymbol{\theta}}$ and $\boldsymbol{\psi}^{\mathrm{T}}\hat{\boldsymbol{\eta}}$ are used to compensate effects of parameter uncertainties and input saturation constraints; $\hat{\boldsymbol{\theta}}$ and $\hat{\boldsymbol{\eta}}$ are estimates of $\boldsymbol{\theta}$ and $\boldsymbol{\eta}$.

Incorporating $\Delta_{\mathrm{f}} = \mathbf{g}_1(\mathbf{x})\boldsymbol{\Phi}^{\mathrm{T}}(\mathbf{x})\boldsymbol{\theta}$, $sat(\mathbf{u}) = \mathbf{u} - \boldsymbol{\psi}^{\mathrm{T}}(\mathbf{x})\boldsymbol{\eta}$ and substituting (13) into (12), it follows

$$\begin{cases} \dot{\mathbf{x}} = [\mathbf{J}(\mathbf{x}) - \mathbf{R}(\mathbf{x})]\nabla H(\mathbf{x}) + \Delta_{\mathrm{f}} - \mathbf{g}_1(\mathbf{x})\boldsymbol{\Phi}^{\mathrm{T}}\hat{\boldsymbol{\theta}} \\ \quad + \mathbf{g}_1(\mathbf{x})[-\mathbf{k}_1\mathbf{g}_1(\mathbf{x})\nabla H_d(\mathbf{x}) + \mathbf{b}^* + \boldsymbol{\psi}^{\mathrm{T}}\hat{\boldsymbol{\eta}} \\ \quad - \mathbf{k}_2(\frac{1}{2}\mathbf{r}^{\mathrm{T}}\mathbf{r} + \frac{1}{2\gamma^2})\mathbf{g}_1(\mathbf{x})\nabla H_d(\mathbf{x})] \\ \quad - \mathbf{g}_1(\mathbf{x})\boldsymbol{\psi}^{\mathrm{T}}\boldsymbol{\eta} + \mathbf{g}_2(\mathbf{x})\mathbf{w} \\ \dot{\hat{\boldsymbol{\theta}}} = \mathbf{Q}\boldsymbol{\Phi}(\mathbf{x})\mathbf{g}_1^{\mathrm{T}}(\mathbf{x})\nabla H_d(\mathbf{x}) \\ \dot{\hat{\boldsymbol{\eta}}} = -\mathbf{P}\boldsymbol{\psi}(\mathbf{x})\mathbf{g}_1^{\mathrm{T}}(\mathbf{x})\nabla H_d(\mathbf{x}) \end{cases} \tag{14}$$

For the first two terms of the first equation in (13) are used to form the closed loop system with new energy function $H_d(\mathbf{x})$, system (14) can be rewritten as

$$\begin{cases} \dot{\mathbf{x}} = [\mathbf{J}(\mathbf{x}) - \mathbf{R}(\mathbf{x})]\nabla H_d(\mathbf{x}) - \mathbf{g}_1(\mathbf{x})\boldsymbol{\psi}^{\mathrm{T}}(\boldsymbol{\eta} - \hat{\boldsymbol{\eta}}) \\ \quad + \mathbf{g}_2(\mathbf{x})\mathbf{w} + \mathbf{g}_1(\mathbf{x})\boldsymbol{\Phi}^{\mathrm{T}}(\boldsymbol{\theta} - \hat{\boldsymbol{\theta}}) \\ \quad + \mathbf{g}_1(\mathbf{x})[-\mathbf{k}_2(\frac{1}{2}\mathbf{r}^{\mathrm{T}}\mathbf{r} + \frac{1}{2\gamma^2})\mathbf{g}_1(\mathbf{x})\nabla H_d(\mathbf{x})] \\ \dot{\hat{\boldsymbol{\theta}}} = \mathbf{Q}\boldsymbol{\Phi}(\mathbf{x})\mathbf{g}_1^{\mathrm{T}}(\mathbf{x})\nabla H_d(\mathbf{x}) \\ \dot{\hat{\boldsymbol{\eta}}} = -\mathbf{P}\boldsymbol{\psi}(\mathbf{x})\mathbf{g}_1^{\mathrm{T}}(\mathbf{x})\nabla H_d(\mathbf{x}) \end{cases} \tag{15}$$

with $H_d(\hat{\boldsymbol{\theta}}) = (\boldsymbol{\theta} - \hat{\boldsymbol{\theta}})\mathbf{Q}^{-1}(\boldsymbol{\theta} - \hat{\boldsymbol{\theta}})$, $H_d(\hat{\boldsymbol{\eta}}) = (\boldsymbol{\eta} - \hat{\boldsymbol{\eta}})\mathbf{P}^{-1}(\boldsymbol{\eta} - \hat{\boldsymbol{\eta}})$.

Using the above results, (15) can be rewritten as

$$\begin{cases} \dot{\mathbf{X}} = [\mathbf{J}(\mathbf{X}) - \mathbf{R}(\mathbf{X})]\nabla H(\mathbf{X}) + \mathbf{G}_2(\mathbf{X})\mathbf{w} \\ \quad = \mathbf{f}(\mathbf{X}) + \mathbf{G}_2(\mathbf{X})\mathbf{W} \\ \mathbf{Y} = \mathbf{C}^{\mathrm{T}}(\mathbf{X})\nabla H(\mathbf{X}) \\ \mathbf{z} = \mathbf{r}(\mathbf{x})\mathbf{G}^{\mathrm{T}}(\mathbf{X})\nabla H_d(\mathbf{X}) \end{cases} \tag{16}$$

where $\mathbf{X} = [\mathbf{x}, \boldsymbol{\theta}, \boldsymbol{\eta}]^{\mathrm{T}}$, $H_d(\mathbf{X}) = H_d(\mathbf{x}) + H_d(\boldsymbol{\theta}) + H_d(\boldsymbol{\eta})$, $\nabla H_d(\mathbf{X}) = [\frac{\partial H_d(\mathbf{X})}{\partial \mathbf{x}}, \frac{\partial H_d(\mathbf{X})}{\partial \boldsymbol{\theta}}, \frac{\partial H_d(\mathbf{X})}{\partial \boldsymbol{\eta}}]^{\mathrm{T}}$, $\mathbf{G}_2 = [\mathbf{g}_2, \mathbf{0}]^{\mathrm{T}}$, $\mathbf{Y} = [\mathbf{y}, \mathbf{0}]^{\mathrm{T}}$, $\mathbf{G}(\mathbf{X}) = [\mathbf{g}_1, \mathbf{0}]^{\mathrm{T}}$, $\mathbf{R}(\mathbf{X}) = diag\{\bar{\mathbf{R}}(\mathbf{x}), \mathbf{0}, \mathbf{0}\}$, $\mathbf{k}_1^{'} = \mathbf{k}_1 + \mathbf{R}(\mathbf{x})$, $\bar{\mathbf{R}}(\mathbf{x}) = \mathbf{R}(\mathbf{x}) + \mathbf{g}_1(\mathbf{x})\mathbf{k}_1^{'}\mathbf{g}_1^{\mathrm{T}}(\mathbf{x}) + \mathbf{g}_1(\mathbf{x})\mathbf{k}_2(\frac{1}{2}\mathbf{r}^{\mathrm{T}}\mathbf{r} + \frac{1}{2\gamma^2})\mathbf{g}_1^{\mathrm{T}}(\mathbf{x})$,

$$\mathbf{C}(\mathbf{X}) = \begin{bmatrix} \mathbf{g}_2(\mathbf{x}) & \mathbf{0} \\ \mathbf{0} & \mathbf{0} \end{bmatrix}, \mathbf{J}(\mathbf{X}) = \begin{bmatrix} \mathbf{J}(\mathbf{x}) & -\mathbf{g}_1\boldsymbol{\Phi}^{\mathrm{T}}\mathbf{Q} & \mathbf{g}_1\boldsymbol{\psi}^{\mathrm{T}}\mathbf{P} \\ \mathbf{Q}\boldsymbol{\Phi}\mathbf{g}_1^{\mathrm{T}} & \mathbf{0} & \mathbf{0} \\ -\mathbf{P}\boldsymbol{\psi}\mathbf{g}_1^{T} & \mathbf{0} & \mathbf{0} \end{bmatrix}.$$

It follows from system (3) and the given disturbance attenuation level γ that if the following conditions are satisfied: (i) system (16) is zero-state detectable [28]; (ii) the inequality holds

$$\tilde{\mathbf{R}}(\mathbf{x}) = \bar{\mathbf{R}}(\mathbf{x}) - \frac{1}{2}\mathbf{g}_1\mathbf{r}^{\mathrm{T}}\mathbf{r}\mathbf{g}_1^{\mathrm{T}} - \frac{1}{2\gamma^2}\mathbf{g}_2\mathbf{g}_2^{\mathrm{T}} \geq \mathbf{0} \tag{17}$$

by the control gain $\mathbf{k}_1$ in $\bar{\mathbf{R}}(\mathbf{x})$. The solution to system (2) can be solved by the proposed control law (13). Note that (17) can be satisfied in the control gain designs.

Here, $V(\mathbf{X}) = H_d(\mathbf{X})$ is chosen as the candidate Lyapunov function since the system's energy function $H_d(\mathbf{X})$ remains positive semi-definite. It is known that $\mathbf{J}(\mathbf{X})$ is skew-symmetric and $\mathbf{R}(\mathbf{X})$ is positive semi-definite. For (16), the Hamiltonian-Jacobi-Isaacs (HJI) inequality may be constructed as

$$\begin{aligned} & \nabla H_d^{\mathrm{T}}(\mathbf{X})\mathbf{f}(\mathbf{X}) + \tfrac{1}{2}h^{\mathrm{T}}(\mathbf{X})h(\mathbf{X}) + \\ & \tfrac{1}{2\gamma^2}\nabla H_d^{\mathrm{T}}(\mathbf{X})\mathbf{G}_2(\mathbf{X})\mathbf{G}_2^{\mathrm{T}}(\mathbf{X})\nabla H_d(\mathbf{X}) \\ =& -\nabla H_d^{\mathrm{T}}(\mathbf{X})\mathbf{R}(\mathbf{X})\nabla H_d(\mathbf{X}) + \\ & \tfrac{1}{2\gamma^2}\nabla H_d^{\mathrm{T}}(\mathbf{X})\mathbf{G}_2(\mathbf{X})\mathbf{G}_2^{\mathrm{T}}(\mathbf{X})\nabla H_d(\mathbf{X}) \\ & + \tfrac{1}{2}\nabla H_d^{\mathrm{T}}(\mathbf{X})\mathbf{G}(\mathbf{X})\mathbf{r}^{\mathrm{T}}\mathbf{r}\mathbf{G}^{\mathrm{T}}(\mathbf{X})\nabla H_d(\mathbf{X}) \\ =& -\nabla H_d^{\mathrm{T}}(\mathbf{x})\bar{\mathbf{R}}(\mathbf{x})\nabla H_d(\mathbf{x}) + \\ & \tfrac{1}{2\gamma^2}\nabla H_d^{\mathrm{T}}(\mathbf{x})\mathbf{g}_2(\mathbf{x})\mathbf{g}_2^{\mathrm{T}}(\mathbf{x})\nabla H_d(\mathbf{x}) \\ & + \tfrac{1}{2}\nabla H_d^{\mathrm{T}}(\mathbf{x})\mathbf{g}_2(\mathbf{x})\mathbf{r}^{\mathrm{T}}\mathbf{r}\mathbf{g}_2^{\mathrm{T}}(\mathbf{x})\nabla H_d(\mathbf{x}) \\ =& -\nabla H_d^{\mathrm{T}}(\mathbf{x})\tilde{\mathbf{R}}(\mathbf{x})\nabla H_d(\mathbf{x}) \leq 0 \end{aligned} \tag{18}$$

Thus, L_2 gain from $\mathbf{w}$ to $\mathbf{z}$ of (16) is no more than γ [28, 31]. And the time derivative of the Lyapunov function $V(\mathbf{X})$ when $\mathbf{w} = \mathbf{0}$ can be presented as

$$\begin{aligned} \dot{V}(\mathbf{X}) &= \dot{H}_d(\mathbf{X}) \\ &= \nabla H_d^{\mathrm{T}}(\mathbf{X})[\mathbf{J}(\mathbf{X}) - \mathbf{R}(\mathbf{X})]\nabla H_d(\mathbf{X}) \\ &= -\nabla H_d^{\mathrm{T}}(\mathbf{X})\mathbf{R}(\mathbf{X})\nabla H_d(\mathbf{X}) \\ &= -\nabla H_d^{\mathrm{T}}(\mathbf{x})\bar{\mathbf{R}}(\mathbf{x})\nabla H_d(\mathbf{x}) \leq 0 \end{aligned} \tag{19}$$

Hence, the system is ensured to be stable when $\mathbf{w} = \mathbf{0}$.

5. Simulation Results

To illustrate the performance of the proposed control, simulations are carried out following the scheme in Fig. 2. Measurements of phase currents, rotor position and motor speed are used as feedback signals for the controller after the specified transformations. Using feedback signals and torque estimates, the control voltages are computed with the law (13). Voltages in the d- and q-axis are used to regulate the inverter.

In Table 1, the parameters of the 3-phase and Y-connected PMSM in the simulations are given.

Control parameters are: $\mathbf{r}(\mathbf{x}) = diag\{0.2, 0.2, 0.2\}$, $\mathbf{k}_1 = [10, 0.07, 0]$, $\mathbf{k}_2 = diag\{1,1,1\}$. It is noted that all control parameters satisfy the condition (17). $\mathbf{b}^*$ is determined by the command. And $\mathbf{P} = diag\{1,1,1\}$, $\mathbf{Q} = diag\{100,1,1\}$,

$$\mathbf{\Phi} = \begin{bmatrix} \frac{0.4}{n_p}(\omega_e - \omega_e^*) & \frac{0.002}{n_p}(\omega_e - \omega_e^*) & 0 \\ \frac{0.002}{n_p}(\omega_e - \omega_e^*) & 0.0001 & 0 \\ 0 & 0 & 0 \end{bmatrix},$$

$$\mathbf{\psi} = \begin{bmatrix} u_d - sat(u_d) & 0 & 50[u_d - sat(u_d)] \\ 0 & 10[u_q - sat(u_q)] & 0 \\ 50[u_d - sat(u_d)] & 0 & 0 \end{bmatrix}$$

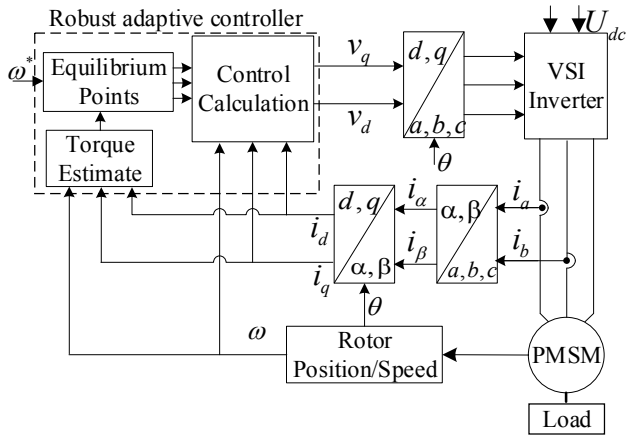

Fig. 2. The scheme of the proposed control

Table 1. Parameters of PMSM

Parameter	Value
Power (kW)	30
Voltage (V)	330
Torque (Nm)	90
Number of poles	8
Stator resistance (Ω)	0.035
d-axis inductance (mH)	0.58
q-axis inductance (mH)	0.58
Flux linkage (Wb)	0.13
Moment of inertia (kgm^2)	2.5×10^{-2}

Remark 3

Determinations of $\mathbf{\Phi}(\mathbf{x})$ and $\mathbf{\psi}(\mathbf{x})$ depend on the objectives, for example to compensate errors caused by uncertainties or input saturations. Therefore, the speed error $\omega_e - \omega_e^*$ is selected as factors of $\mathbf{\Phi}(\mathbf{x})$ and the control input errors $u_i(\mathbf{x}) - sat(u_i(\mathbf{x}))$ $(i = d, q)$ are chosen for $\mathbf{\psi}(\mathbf{x})$. $sat(u_i)$ is determined using (6).

5.1 Simulations under nominal parameters

To test the validity of the control, the speed tracking using the proposed approach is compared with that of IDA. The speed tracking, errors and load torque estimation required in the control are shown in Fig. 3 (a) and (b). Comparisons show that both methods are effective to estimate and track the references under nominal conditions.

Fig. 4 (a) show that the current in d-axis goes to zero as expected, and q-axis current produces electromagnetic

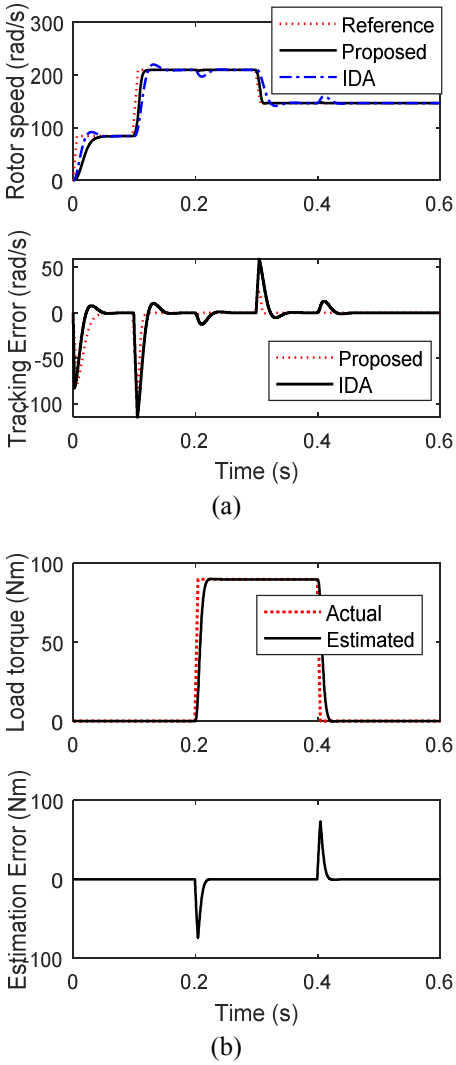

Fig. 3. Comparisons of speed tracking and load estimation: (a) speed tracking and errors; (b) load estimation and error

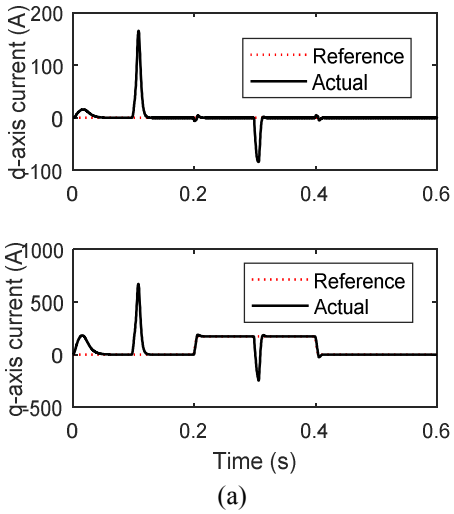

(a)

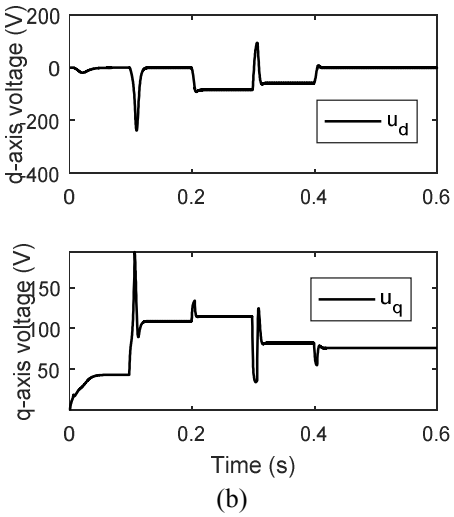

(b)

Fig. 4. Current responses and voltage actions: (a) d- and q-axis currents; (b) d- and q-axis voltages

torque to counteract the load. Fig. 4 (b) shows that the controller reacts according to the command or external load.

5.2 Simulations under disturbances

To test the robustness of the proposed control, variations of electrical parameters (R_s, L_d, L_q, ψ) and mechanical parameters (J_m, B) are set to 10%. And a disturbance $[\sin(50\pi t), \sin(10\pi t), \sin(100\pi t)]$ is added.

Fig. 5 presents the speed responses and tracking error of both the proposed approach and IDA method under electrical parameter uncertainties. As shown, the speed tracking errors using the proposed control converge to zero. And compared to the results of the traditional IDA control which doesn't incorporate adaptive compensations, the steady-state error of the proposed control is reduced. The speed responses under mechanical parameter uncertainties are shown in Fig. 6. As depicted, the speed response using the proposed control converges to its reference and the steady-state error is smaller than that of the traditional IDA control.

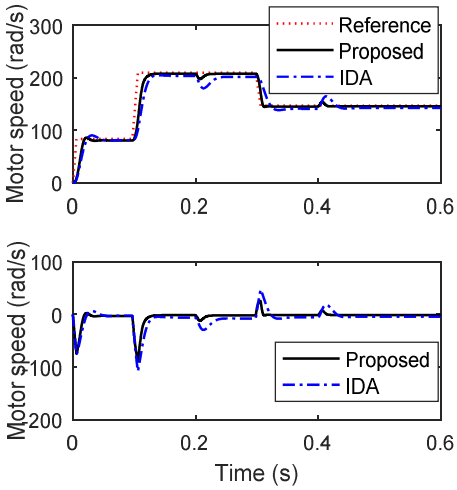

Fig. 5. Speed tracking and errors under electrical parameter uncertainties

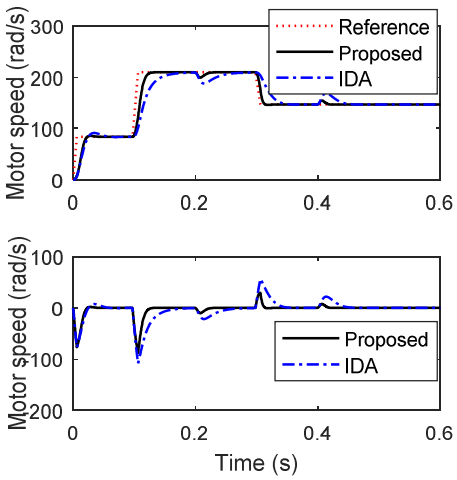

Fig. 6. Speed tracking and errors under mechanical parameter uncertainties

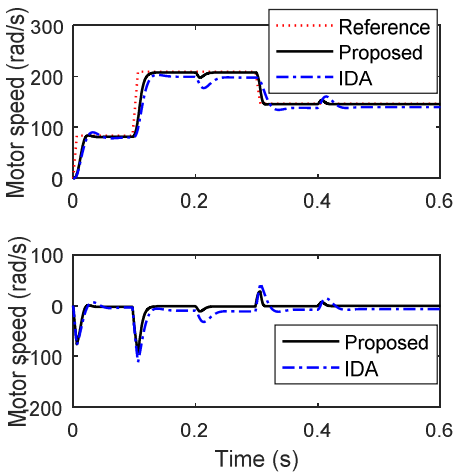

Fig. 7. Speed tracking and errors under electrical and mechanical parameter uncertainties

Fig. 7 gives the speed regulation and tracking errors of

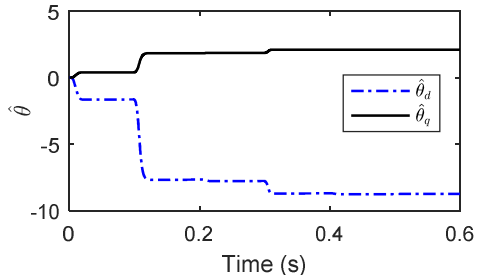

Fig. 8. Transient responses of $\hat{\theta}$

Table 2. Statistics of the speed tracking errors under mechanical uncertainties (1), electrical uncertainties (2), mechanical and electrical uncertainties (3)

Methods	Maximum error	Average error	Standard deviation
Proposed (1)	88.9496	-4.3807	0.0815
IDA (1)	106.2846	-7.4720	0.0862
Proposed (2)	87.0842	-3.5631	0.0871
IDA (2)	106.4080	-3.6520	0.0731
Proposed (3)	91.8960	-4.2840	0.0810
IDA (3)	109.1420	-10.1930	0.1176

both methods under electrical and mechanical uncertainties. It is shown in that the speed response using the proposed approach tracks its reference despite uncertainties, and its error is smaller than that of the IDA control. The results reveal that the proposed control performs effectively to achieve speed regulation when motor parameters change.

The statistics of the tracking error is given in Table 2. As shown, the proposed approach performs better than IDA.

As shown in Fig. 8, as an adaptive compensation action in the proposed control, $\hat{\theta}$ reacts to cancel the offset due to parameter variations. The estimation enables the proposed control to act accordingly to reduce the steady-state error and achieve better tracking. And it is shown that the stability and regulation are preserved even if uncertainties deteriorate the performance of the control system.

5.3 Simulations under input saturations

To demonstrate the effectiveness and advantages of handling the uncertainties and saturation constraints, the proposed approach is compared with the IDA control without input constraints (Traditional IDA) and the PI anti-windup control. The proportional and integral gains of the PI control for d-, q-axis currents and speed loop are: 1, 0.1; 1, 0.1; 25, 40, respectively.

Results are presented in Fig. 9. As shown in Fig. 9(a), the speed tracking using the proposed control converges to its reference and the error attenuates to zero. Fig. 9(b) shows that current responses follow the references. Fig. 9 (c) shows that the control inputs of the proposed control, which are limited by the boundaries, are constrained by the given limits. The results mean that the control operates as predicted for the saturation compensations.

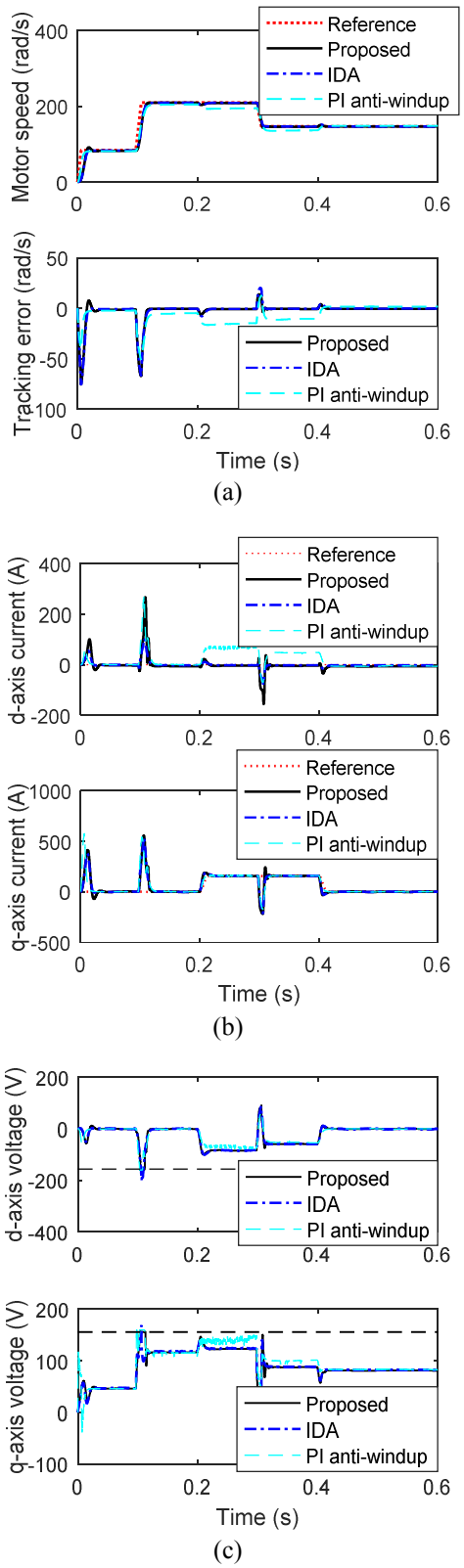

Fig. 9. Responses under uncertainties and saturations: (a) speed responses and errors; (b) current responses; (c) voltage **u** and saturated voltage *sat*(**u**).

The comparison statistics is given in Table 3. The results show that the average error and standard deviation of the

Table 3. Statistics of the speed tracking errors

Errors	Maximum	Average	Standard
Proposed	75.3841	-3.4036	0.0434
Traditional IDA	76.0038	-4.9816	0.1443
PI anti-windup	50.9220	-5.4489	0.1587

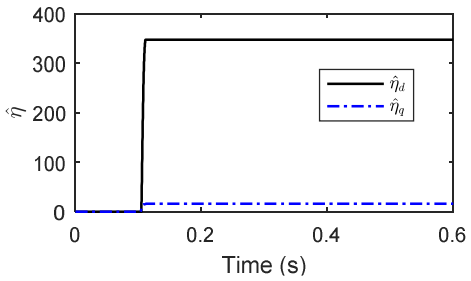

Fig. 10. Transient responses of $\hat{\eta}$.

proposed approach are smaller. This is mainly because the control can compensate the effects of uncertainties and saturations to achieve better steady performance.

Transient behaviors of $\hat{\eta}$, when the saturations occur, are presented in Fig. 10. As shown, the proposed control works effectively to regulate the control inputs in the presence of uncertainties and saturations and reacts simultaneously to keep the voltages within the limits. This reveals that the designed control performs well to counteract the saturation effects.

6. Conclusion

A robust adaptive control has been presented for the speed regulation of PMSM considering parameter uncertainties, external perturbations and input saturations. A nonlinear adaptive control is designed to handle the effects of uncertainties and saturations. And then a new robust adaptive strategy is put forward by combining the adaptive control with the nonlinear robust technique. Stability of system has been ensured involving the saturated control inputs. Simulations results confirmed the effectiveness of the proposed approach. The average and standard deviation of the tracking error are at least 32% and 70% smaller than the compared methods.

References

[1] H. Jun, H. Ahn, H. Lee, S. Go and J. Lee, "A maximum power control of IPMSM with real-time parameter identification," *J. Electr. Eng. Technol*., vol. 12, no. 1, pp. 110-116, Jan. 2017.

[2] L. Sun, Y. Wang, and G. Feng, "Control design for a class of affine nonlinear descriptor systems with actuator saturation," *IEEE Trans. Autom. Control*, vol. 60, no. 8, pp. 2195-2200, Aug. 2015.

[3] A. Wei, Y. Wang, and X. Hu, "Parallel simultaneous stabilization of a set of port-controlled Hamiltonian systems subject to actuator saturation," *J. Syst. Sci. Complex*., vol. 24, no. 1, pp. 120-139, Aug. 2011.

[4] Q. Zhou, H. Li, C. Wu, L. Wang, and C. Ahn, "Adaptive fuzzy control of nonlinear systems with unmodeled dynamics and input saturation using small-gain approach," *IEEE Trans. Syst. Man, Cybern.: Syst*., vol. 47, no. 8, pp. 1979-1989, Aug. 2017.

[5] A. Donaire and S. Junco, "On the addition of integral action to port-controlled Hamiltonian systems," *Automatica*, vol. 45, pp. 1910-1916, Jun. 2009.

[6] V. Petrovic, R. Ortega, and A. Tankovic, "Interconnection and damping assignment approach to control of permanent magnet synchronous motors," *IEEE Trans. Control Syst.Technol*., vol. 9, no. 6, pp. 811-820, Nov. 2011.

[7] T. Türker, B. Umit, and B. Faruk, "A robust predictive current controller for PMSM drives," *IEEE Trans. Ind. Electron*., vol. 63, no. 6, pp. 3906-3914, Jan. 2016.

[8] S. Garin and N. Mohmed, "MTPA- and FW-based robust nonlinear speed control of IPMSM drive using Lyapunov stability criterion," *IEEE Trans. Ind. Appl*., vol. 52, no. 5, pp. 4365-4374, Sep./Oct. 2016.

[9] A. Vahid, F. Ahmed, and M. Menhaj, "Position and current control of an interior permanent-magnet synchronous motor by using loop-shaping methodology: blending of H_∞ mixed-sensitivity problem and T-S fuzzy model scheme," *ASME J. Dyn. Syst., Measurement, Control*, vol. 135, pp. 1-11, Sep. 2013.

[10] V. Azimi, M. Nekoui, and A, Fakharian, "Robust multi-objective H_2/H_∞ tracking control based on T-S fuzzy model for a class of nonlinear uncertain drive systems," *Proc. IMechE. Part I: J. of Syst. Control Eng*., vol. 226, no. 8, pp. 1107-1118, Jun. 2012.

[11] N. Vu, H. Choi, R. Kim, and J. Jung, "Robust speed control method for permanent magnet synchronous motor," *IET Electr. Power Appl*., vol. 6, iss. 7, pp. 399-411, Aug. 2012.

[12] L. Guo and L. Parsa, "Model reference adaptive control of five-phase IPM motors based on neural network," *IEEE Trans. Ind. Electron*., vol. 59, no. 3, pp. 1500-1508, Mar. 2012.

[13] A. Khan, N. Uddin, and A. Rahman, "A novel wavelet- neural-network-based robust controller for IPM motor drives," *IEEE Trans. Ind. Electron*., vol. 49, no. 5, pp. 2341-2351, Sep./Oct. 2013.

[14] P. Tomi and J. Chiasson, "A nonlinear adaptive speed tracking control for sensorless permanent magnet step motors with unknown load torque," *Int. J. Adaptive Control and Signal Process*., vol. 22, pp. 266-288, Jun. 2007.

[15] F. El-Sousy, "Robust adaptive H_∞ position control via a wavelet-neural-network for a DSP-based permanent-magnet synchronous motor servo drive

system," *IET Electr. Power Appl*., vol. 4, iss. 5, pp. 333-347, May 2010.
[16] F. El-Sousy, "Robust wavelet-neural-network sliding-mode control system for permanent magnet synchronous motor drive," *IET Electr. Power Appl*., vol. 5, iss. 1, pp. 113-132, Jan. 2011.
[17] M. Rehan, M. Tufail, C. Ahn, and M. Chadli, "Stabilisation of locally Lipschitz non-linear systems under input saturation and quantisation," *IET Control Theory & Appl*., vol. 11, iss. 9, pp. 1459-1466, Mar. 2017.
[18] J. Chio and S. Lee, "Antiwindup strategy for PI-type speed controller," *IEEE Trans. Ind. Electron*., vol. 56, no. 6, pp. 2039-2046, Jun. 2009.
[19] H. Shin and J. Park, "Anti-windup PID controller with integral state predictor for variable-speed motor drives," *IEEE Trans. Ind. Electron*., vol. 56, no. 3, pp. 1509-1516, Mar. 2012.
[20] R. Errouissi, M. Ouhrouche, W. Chen, A. Trzynadlowski, "Robust cascaded nonlinear predictive control of a permanent magnet synchronous motor with antiwindup compensator," *IEEE Trans. Ind. Electron*., vol. 59, no. 8, pp. 3078-3088, Aug. 2012.
[21] R. Errouissi, M. Ouhrouche, and W. Chen, "Robust nonlinear generalized predictive control of a permanent magnet synchronous motor with an anti-windup compensator," in Proc. *IEEE Int. Symposium Ind. Electron*., 2010, pp. 3184-3189.
[22] Y. Guo, Z. Xi, and D. Cheng, "Speed Regulation of permanent magnet synchronous motor via feedback dissipative Hamiltonian realization," *IET Control Theory Appl*., vol. 1, no. 1, pp. 281-290. Jan. 2007.
[23] Y. Zhao and L. Dong, "Robust speed control of a permanent magnet synchronous motor system," *in Proc. 28th CDC Conf*., 2016, pp. 3271-3276.
[24] R. Ortega and C. Eloisa, "Interconnection and damping assignment passivity control: a survey," *Eur. J. Control*, vol. 10, pp. 432-450, Jun. 2013.
[25] A. Dirksz and A. Scherpen, "Structure preserving adaptive control of port-Hamiltonian systems," *IEEE Trans. Autom. Control*, vol. 57, no. 11, pp. 2880-2884, Nov. 2012.
[26] A. Wei and Y. Wang, "Adaptive parallel simultaneous stabilization of a set of uncertain port-controlled Hamiltonian systems subject to actuator saturation," *Int. J. Adaptive Control and Signal Process*., vol. 28, no. 11, pp. 1128-1144, Sep. 2013.
[27] A. Wei and Y. Wang, "Stabilization and H_∞ control of nonlinear port-controlled Hamiltonian systems subject to actuator saturation," *Automatica*, vol. 46, pp. 2008-2013, Aug. 2010.
[28] A. Van der Schaft, L_2-Gain and Passivity Techniques in Nonlinear Control, Berlin: Springer, 1999.
[29] C. Lin and T. Liu, "Chattering free robust nonlinear controller for an interior permanent magnet synchronous motor speed drive system," *in Proc. 36th Annual Conf. IEEE Ind. Electron. Soc*., 2010, pp. 2218-2223.
[30] M. Aliyu, Nonlinear H_∞ Control, Hamiltonian Systems and Hamilton-Jacobi Equations, New York: CRC Press, 2011.
[31] Y. Orlov and L. Aguilar, Advanced H_∞ Control: Towards Nonsmooth Theory and Applications, New York: Springer, 2014.

Shaofang Wu He is a Ph.D. candidate with National Engineering Laboratory for Automotive Electronics and Control Technology in Shanghai Jiaotong University, Shanghai, China. His research interests focus on electric vehicle and drive control.

Jianwu Zhang He is a full professor with National Engineering Laboratory for Automotive Electronics and Control Technology in Shanghai Jiaotong University, Shanghai, China. His research interests focus on electric vehicles, transmission and drive systems.